# Mechanisms of Silicon Surface Passivation by Negatively Charged Hafnium Oxide Thin Films

Ailish Wratten, Sophie L. Pain, David Walker, Arne Benjamin Renz, Edris Khorani, Tim Niewelt, Nicholas E. Grant, and John D. Murphy

***Abstract*—We have studied the mechanisms underpinning effective surface passivation of silicon with hafnium oxide ($HfO_2$) thin films grown *via* atomic layer deposition (ALD). Plasma-enhanced ALD with $O_2$ plasma and a tetrakis(dimethylamido)hafnium precursor was used to deposit 12 nm thick $HfO_2$ films at 200 °C on high-lifetime 5 Ωcm *n*-type Czochralski silicon wafers. The passivation was activated by postdeposition annealing, with 30 min in air at 475 °C found to be the most effective. High-resolution grazing incidence X-ray diffraction measurements revealed the film crystallized between 325 and 375 °C, and this coincided with the onset of good passivation. Once crystallized, the level of passivation continued to increase with higher annealing temperatures, exhibiting a peak at 475 °C and yielding surface recombination velocities of $<5$ cm s$^{-1}$ at $5 \times 10^{14}$ cm$^{-3}$ injection. A steady decrease in effective lifetime was then observed for activation temperatures $>475$ °C. By superacid repassivation, we demonstrated this reduction in lifetime was not because of a decrease in the bulk lifetime, but rather because of changes in the passivating films themselves. Kelvin probe measurements showed the films are negatively charged. Corona charging experiments showed the charge magnitude is of order $10^{12}$ qcm$^{-2}$ and that the reduced passivation above 475 °C was mainly because of a loss of chemical passivation. Our study, therefore, demonstrates the development of highly charged $HfO_2$ films and quantifies their benefits as a standalone passivating film for silicon-based solar cells.**

***Index Terms*—Atomic layer deposition (ALD), hafnium oxide ($HfO_2$), lifetime, silicon, surface passivation.**

## I. Introduction

HIGH-QUALITY surface passivation plays an essential role in the operation of high-efficiency silicon photovoltaic cells. Passivation is achieved by deposition or growth of a dielectric thin film, which suppresses surface recombination by terminating dangling bonds (chemical passivation) and/or by repelling carriers away from surfaces by a built-in charge (field effect passivation). A variety of such films have been researched [1] and from the perspective of commercial silicon photovoltaics, $Al_2O_3$ grown by atomic layer deposition (ALD) and $SiN_x$ grown by plasma-enhanced chemical vapor deposition (PECVD) are the most commonly used at present.

Hafnium oxide ($HfO_2$) is a dielectric that has been extensively researched by the electronics industry for applications in transistors and capacitors [2], [3]. It has also been investigated for applications as a protective barrier layer, demonstrating resistance to oxidation, copper corrosion, and general weathering [4], [5], [6]. $HfO_2$ has the potential to become a useful passivation layer for photovoltaics as it can be grown by established ALD processes and can have either positive or negative charge polarity [7], [8], [9], [10], [11], [12], [13]. The benefits of $HfO_2$ as a passivation layer are especially apparent for ultrathin films below 5 nm, where it has been shown to outperform $Al_2O_3$ [14]. This advantage suggests a potential application for $HfO_2$ films in passivating contact structures.

In common with most ALD-based passivation schemes, a postdeposition anneal is required to "activate" the passivation by $HfO_2$. Previous investigations have been conducted on both the deposition parameters, including precursors, deposition temperatures, and cycles [7], [11], [12], as well as the postdeposition annealing conditions [11], [12], [13] for $HfO_2$. Most studies find $HfO_2$ passivation to give a surface recombination velocity (SRV) of 3–5 cm/s [11], [13], although some studies have claimed as low as 1.2 cm/s [12]. Most passivation studies have been performed on float-zone (FZ) silicon substrates, which have been shown to degrade at the temperatures necessary to activate the $HfO_2$ passivation [15]. We instead use Czochralski (Cz) silicon, which is the material of choice for the photovoltaics industry. Importantly, our study includes a room temperature superacid repassivation process after $HfO_2$ passivation. This enables us to separate changes in surface recombination from those in bulk recombination, which has not been done in previous studies.

The aim of our study is to establish the mechanisms of the activation process necessary to achieve good levels of passivation from $HfO_2$ thin films. We have therefore complemented charge carrier lifetime investigations with high-resolution X-ray diffraction (XRD), Kelvin probe, and corona charging, which

Manuscript received 30 June 2022; revised 31 October 2022 and 30 November 2022; accepted 1 December 2022. Date of publication 20 December 2022; date of current version 12 January 2023. The work of A. Wratten and S. L. Pain was supported by EPSRC studentships (EP/R513374/1). This work was supported in part by the EPSRC COIL Project (EP/V037749/1) and in part by the Leverhulme Trust Research Project Grant (RPG-2020-377). *(Corresponding author: John D. Murphy.)*

Ailish Wratten, Sophie L. Pain, Arne Benjamin Renz, Edris Khorani, Nicholas E. Grant, and John D. Murphy are with the School of Engineering, University of Warwick, Coventry CV4 7AL, U.K. (e-mail: ailish.wratten@warwick.ac.uk; sophie.pain@warwick.ac.uk; a.renz@warwick.ac.uk; edris.khorani@warwick.ac.uk; nicholas.e.grant@warwick.ac.uk; john.d.murphy@warwick.ac.uk).

David Walker is with the Department of Physics, University of Warwick, Coventry CV4 7AL, U.K. (e-mail: d.walker.2@warwick.ac.uk).

Tim Niewelt is with the School of Engineering, University of Warwick, Coventry CV4 7AL, U.K., also with the Fraunhofer Institute for Solar Energy Systems ISE, 79110 Freiburg, Germany, and also with the Institute for Sustainable Systems Engineering, University of Freiburg, 79110 Freiburg, Germany (e-mail: tim.niewelt@warwick.ac.uk).

Color versions of one or more figures in this article are available at https://doi.org/10.1109/JPHOTOV.2022.3227624.

Digital Object Identifier 10.1109/JPHOTOV.2022.3227624

This work is licensed under a Creative Commons Attribution 4.0 License. For more information, see https://creativecommons.org/licenses/by/4.0/

provides an in-depth understanding of the physical and electrical characteristics of the $HfO_2$ films. These investigations give insight into the postdeposition treatments necessary to maximize the overall $HfO_2$ passivation quality, distinguishing between the contributions of chemical and field-effect passivation.

## II. Experimental Methods

Lifetime samples were fabricated from chemically etched 120 μm thick 5 Ωcm *n*-type Cz-Si (100)-orientation wafers, cut into 5 × 5 cm squares. Lifetime optimization was performed on the same batch of wafers to minimize variations between batches. A separate batch of samples was used for the corona charging measurements and these samples were nominally identical except for being 150 μm thick. The samples used for the XRD measurements were thicker, mirror-polished silicon substrates. Before ALD, all samples were first subjected to a rigorous cleaning and etching process developed previously [16]. This involves submerging the samples in a "standard clean 1" (SC1) solution (500 ml de-ionized (DI) $H_2O$, 100 ml $NH_4OH$ (30%), 100 ml $H_2O_2$ (30%)) for 10 min, followed by a "standard clean 2" (SC2) solution (500 ml DI $H_2O$, 100 ml HCl (37%), 100 ml $H_2O_2$ (30%)) for 10 min. Both solutions were heated to 80 °C, with the $H_2O_2$ being added once the solutions were up to temperature. Between these two steps, the samples were immersed in a 25% tetramethylammonium hydroxide (TMAH) solution for 10 min, again heated to 80 °C. A DI water rinse and 60 s dip in a 1% HF solution (490 ml DI $H_2O$, 10 ml 50% HF) were conducted before each cleaning and etching step. After final DI water rinse the wafers were individually dipped in a solution of 2% HF until they pulled dry, before immediately being placed onto the ALD stage.

A Veeco Fiji G2 system was used for the plasma-enhanced ALD of $HfO_2$ at 200 °C with an $O_2$ plasma and tetrakis(dimethylamido)hafnium (TDMAH) used as the co-reactant and precursor, respectively. Argon was used as the inert purge gas. TDMAH was pulsed into the chamber for 0.25 s, followed by a 6 s pulse of $O_2$ plasma at 300 W. A 5 s purge was conducted before and after each step. For all samples, 100 process cycles were performed per side, which was later confirmed by X-ray reflectivity (XRR) to give a film thickness of 12 nm. For some experiments, $Al_2O_3$ passivation was used for control purposes, which was also deposited at 200 °C by plasma-enhanced ALD. The precursors used for $Al_2O_3$ were trimethylaluminium (TMA) and $O_2$ plasma, with argon again used as the purge gas. For this recipe, the TMA was pulsed into the chamber for 0.06 s, followed by a 6 s pulse of $O_2$ plasma at 300 W, with a 4 s purge after each precursor. In total, 160 cycles of this process were completed, resulting in a film thickness of 20 nm. After ALD, samples were annealed *ex situ* in a tube furnace with the times chosen in the range 2 to 60 min and the temperatures up to 625 °C. The ambient was air unless otherwise specified.

The effective lifetime of the coated and annealed samples was measured by transient photoconductance decay using a Sinton WCT-120 lifetime tester. Lifetimes were assumed to be accurate to ±10% guided by the work of Blum et al. [17]. This was then used to calculate SRV according to

$$SRV = \frac{W}{2}\left(\frac{1}{\tau_{eff}} - \frac{1}{\tau_{bulk}}\right) \quad (1)$$

where $W$ is the substrate thickness, $\tau_{eff}$ is the effective lifetime, and $\tau_{bulk}$ is the bulk lifetime. We have assumed that there is no other bulk recombination and, thus, $\tau_{bulk}$ is the intrinsic lifetime ($\tau_{intrinsic}$) which we take from the work in [18]. Consequently, our values of SRV should be regarded as upper limits. We also calculated the recombination parameter, $J_0$, using the Sinton Instruments Lifetime Software (version 4.5.2), through application of a similar approach to Kane and Swanson [19]. We have reported single-sided $J_0$ values, which are half of the extracted $J_0$ values.

To isolate potential bulk and surface degradation effects, certain samples were stripped of their $HfO_2$ passivation and repassivated with a temporary superacid scheme [16], [20], [21]. This is known to provide very good surface passivation (SRV <1 cm/s) without modifying the sample's bulk lifetime because of temperature or hydrogenation effects. $HfO_2$ films were stripped by immersion in a 10% HF solution until the surface became hydrophobic, then cleaned and etched once again as described previously. The samples were then dipped in a solution of bis(trifluoromethanesulfonyl)amide (TFSA) in pentane (2 mg/ml) for 1 min to create the temporary surface passivation before lifetime measurements were made. TFSA and pentane (purity ≥95.0% and >99%, respectively) were obtained from Sigma-Aldrich.

Grazing incidence XRD (GI-XRD) was carried out on annealed, $HfO_2$-coated, mirror-polished wafers using a third-generation Panalytical Empyrean XRD Diffractometer, equipped with multicore (iCore, iCore) optics and a Pixcel3D detector under Cu $K_{\alpha 1/2}$ radiation. Peaks were fitted using the Panalytical XRD crystallography data analysis software HighScore Plus and verified using GSAS-II [22]. Film thickness was obtained by analyzing XRR data with Panalytical's AMASS software, and this was confirmed by a Filmetrics F40 reflectometry measurement tool.

Contact potential difference (CPD) and surface photovoltage (SPV) were measured using a KP Technology SKP5050 Kelvin probe system, with a 2 mm diameter gold-plated tip, following the method of Baikie et al. [23]. An effective work function was calculated from the CPD using a gold reference sample and the SPV was measured by cycling through 50 data points in the dark and 50 data points under illumination, taken every 0.5 s. A Fiber-Lite DC-950 quartz tungsten halide lamp was used for sample illumination, with a light intensity of 12.2 W/cm$^2$ at 635 nm, measured by a Thorlabs PM16-130 power meter. SPV was determined as the difference between the averaged dark and light values.

Corona charging was used to investigate the magnitude of bulk charge within the $HfO_2$ films. Positive charge was deposited onto the surface of the $HfO_2$ layer through use of a custom-built setup composed of a needle positioned 7 cm above the sample and held at approximately 7 kV for 5 s on each side of the sample. Charge deposition was calibrated *via* a Kelvin probe method proposed by Bonilla et al. [24] and [25].

## III. Results and Discussion

### A. Variation of Activation Annealing Conditions

We first present the results of a study to optimize the post-ALD activation conditions for $HfO_2$ surface passivation. Fig. 1 shows results for optimization of annealing ambient and time. In Fig. 1(a), effective lifetime curves are shown for $HfO_2$ and $Al_2O_3$ annealed at 475 °C in different ambients (air, $N_2$, and Ar). Two curves are shown for each condition to give an indication of process reproducibility. Annealing in air gave the best results for both $HfO_2$ and $Al_2O_3$; $N_2$ and Ar annealing resulted in marginally worse performance for $Al_2O_3$ and considerably worse performance for $HfO_2$. Based on these results, air was used as the postdeposition annealing ambient for the rest of this study.

The effect of annealing time on measured lifetime for $HfO_2$ annealed at 475 °C in air for different times is shown in Fig. 1(b) and (c). The effective lifetime values (and hence the passivation levels) initially increase with time up to 25 min and, after this time, no further improvements occur. There is no obvious degradation in the measured lifetimes at longer annealing times, indicating there is a broad temporal process window for thermal activation. Based upon these results, subsequent experiments in this article used an annealing time of 30 min.

Results for the temperature dependence of the activation of the $HfO_2$ passivation with isochronal 30 min annealing in air are shown in Fig. 2. Effective lifetimes in samples annealed below 300 °C were too low to measure reliably. Effective lifetime increases with temperature up to 475 °C, then decreases at higher temperatures. We have plotted the lifetime curves systematically increasing up to 475 °C in Fig. 2(a) and systematically decreasing at higher temperatures up to 625 °C in Fig. 2(b). SRV values extracted at an excess carrier density of $5 \times 10^{14}$ cm$^{-3}$ are shown in Fig. 2(c), with the minimum value of 4.1 cm/s determined at 475 °C. This value is significantly lower than initial investigations into $HfO_2$ passivation [9], but is in line with more recently published results by Cui et al. [11] and Tomer et al. [13] who achieved SRV values of 3.3 cm/s and 5 cm/s, respectively. Direct comparison between literature SRV values is not always possible because of the influence of doping concentration [26], but these comparisons have been made between Si wafers with similar resistivities (in the 1–5 Ωcm range). $J_0$ values are also plotted in Fig. 2(c), with a value of 37.1 fA/cm$^2$ at 475 °C and a minimum of 28.4 fA/cm$^2$ at 500 °C. There is a lack of direct reporting of $J_0$ values for $HfO_2$ passivated surfaces in the literature, but one recent paper reports values an order of magnitude higher than ours [27].

### B. Superacid Repassivation to Distinguish Between Bulk and Surface Effects

As the effective lifetime is determined by competing bulk and surface effects, it is important to ascertain whether bulk or surface (or both) effects are responsible for the activation temperature dependence shown in Fig. 2. This balance was not considered in prior studies of $HfO_2$ passivation [10], [11], [12], [13]; therefore, it has not yet been proven that there is a

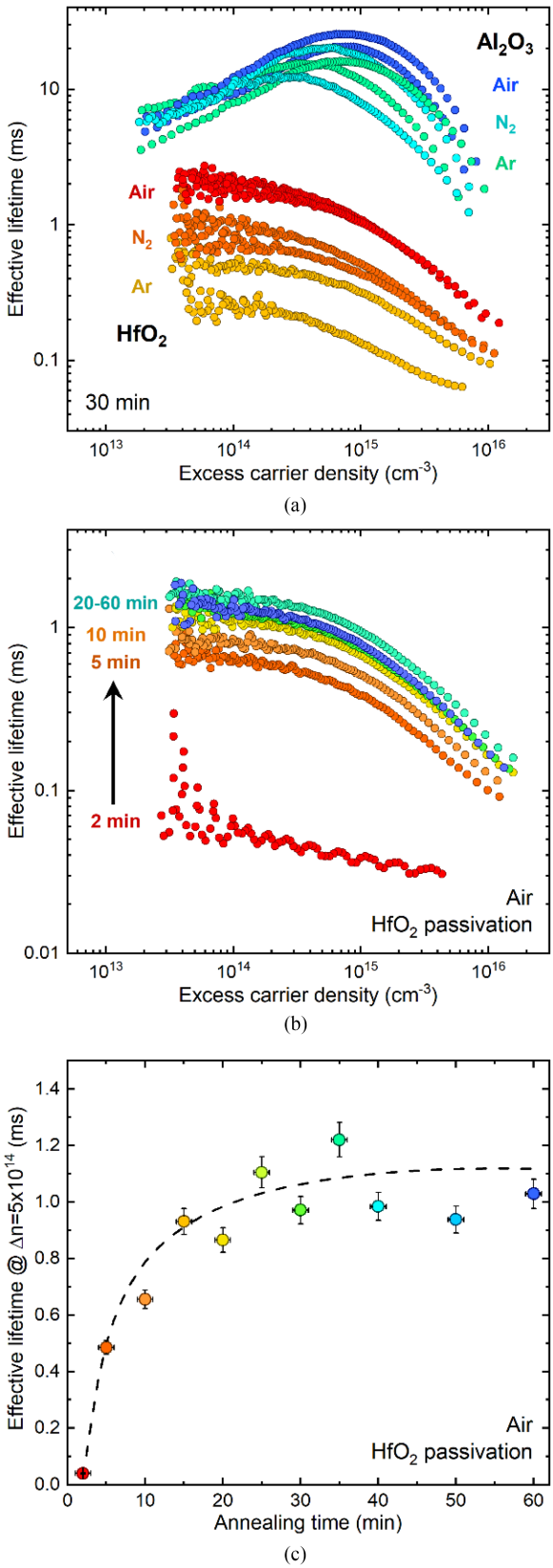


Fig. 1. (a) Lifetime curves for 120 µm thick 5 Ωcm *n*-type Cz-Si wafers coated with $HfO_2$ and $Al_2O_3$ films annealed in various ambients at 475 °C. (b) Lifetime curves for identical wafers coated with 12 nm $HfO_2$ films annealed in air at 475 °C for different lengths of time. (c) Effective lifetimes at an excess carrier density of $5 \times 10^{14}$ cm$^{-3}$ for each annealing time in (b) with the dashed curve providing a guide to the eye.

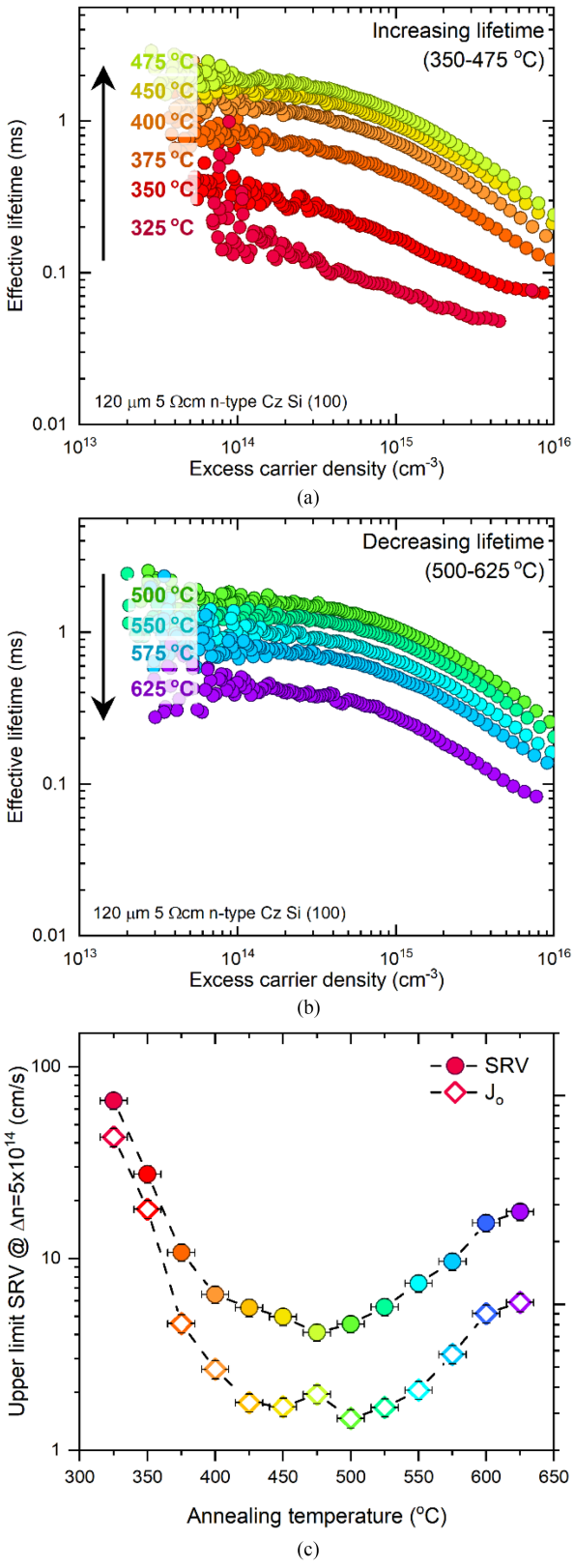


Fig. 2. (a) Lifetime curves for 12 nm (100 cycles) of ALD deposited $HfO_2$ films on 120 µm 5 Ωcm *n*-type Cz-Si wafers, annealed at various temperatures (300–475 °C) for 30 min. (b) Lifetime curves of the same type of samples annealed at higher temperatures (500–625 °C) for 30 min. (c) Upper limit SRV values calculated using (1) at an excess carrier density of $5 \times 10^{14}$ cm$^{-3}$ and single-sided $J_0$ values [19] plotted as a function of activation temperature.

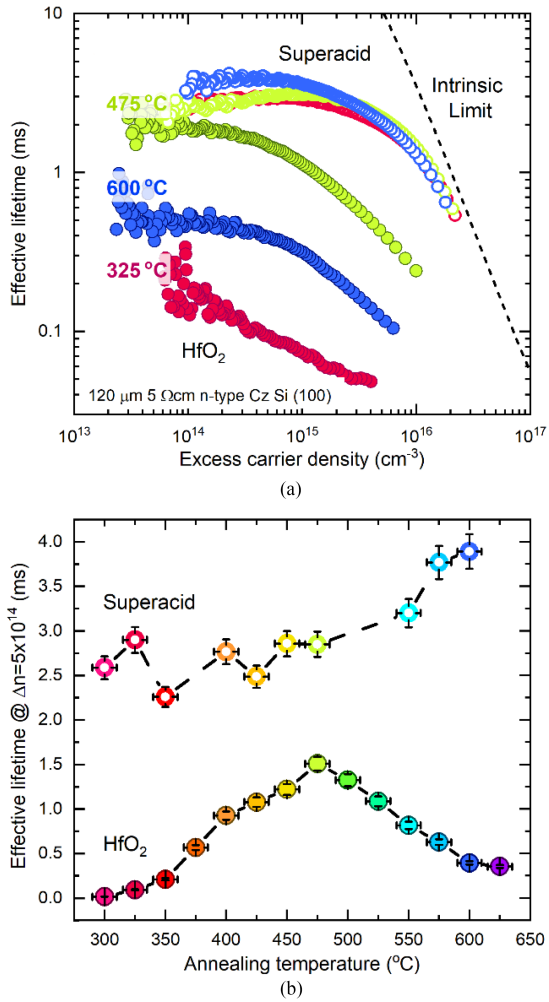


Fig. 3. (a) Lifetime curves for selected $HfO_2$ passivated samples activated at the temperatures shown, together with lifetime curves for the same samples after $HfO_2$ removal and superacid repassivation. The intrinsic limit of Niewelt et al. [18] is also plotted. (b) Comparison between effective lifetimes measured on 120 µm thick 5 Ωcm *n*-type Cz-Si samples passivated with 12 nm (100 cycles) of ALD-deposited $HfO_2$ *versus* a TFSA superacid solution, taken at an excess carrier density of $5 \times 10^{14}$ cm$^{-3}$.

peak temperature for $HfO_2$ passivation activation. By removing the $HfO_2$ passivation and repassivating the samples with a temporary superacid-based passivation scheme we were able to measure the effective lifetime consistently with the same surface recombination level to deduce information on the bulk lifetime.

Fig. 3(a) compares the lifetime curves of samples coated with $HfO_2$ and the same samples when repassivated with the superacid-based approach after being subjected to activation anneals at three different temperatures: 325 °C, 475 °C, and 625 °C. Effective lifetimes are higher with superacid passivation since this approach provides a short-term SRV $< 1$ cm/s [16], [20], [21] which is better than the investigated $HfO_2$ layers. The difference in injection dependence between the $HfO_2$ and superacid curves is likely caused by the lower concentration of fixed charges with the superacid passivation [21], [28]. The injection dependence of the superacid passivated samples is relatively consistent, irrespective of the thermal history of the sample.

Fig. 3(b) shows a comparison in effective lifetime between $HfO_2$ passivated and superacid passivated samples, extracted at an excess carrier density of $5 \times 10^{14}$ $cm^{-3}$. With superacid-passivation, no reduction in effective lifetime was found to occur above 475 °C, which demonstrates that the reduction in effective lifetime at higher activation temperatures with $HfO_2$ is not because of bulk lifetime degradation.

In fact, there is a slight increase in effective lifetime for higher annealing temperatures which may be because of thermal deactivation of recombination centers within the silicon bulk [29], [30]. This shows that the cause of the decline in effective lifetimes at higher temperatures shown in Fig. 2(b) is not related to the bulk of the material, but rather because of a decline in passivation from the $HfO_2$ films.

Comparing this work to the literature, we see a similar trend in annealing temperature dependence in the work of Cheng et al. [10] who also used Cz-Si in their investigations and found a peak in effective lifetime at 450 °C. Other works, however, have demonstrated peaks in $HfO_2$ passivation at significantly lower temperatures. Gougam et al. [12] found their lifetimes to peak at 400 °C and Cui et al. [11] reached a minimum SRV value at 350 °C. Importantly, these papers used FZ-Si in their investigations, which has been shown to often be prone to degradation above these temperatures [16], [31]. As such, the temperature dependence of the activation of $HfO_2$ passivation shown in publications using FZ-Si may have been influenced by the effect of bulk degradation. Consequently, we believe it is likely that studies using FZ-Si underestimate the activation temperature required to optimize passivation from $HfO_2$ films.

### C. Film Crystallinity

GI-XRD measurements were taken to investigate any potential correlation between the passivation quality and film crystallinity of the $HfO_2$ films. Fig. 4(a) shows the XRD patterns for 12 nm $HfO_2$ films annealed with the same conditions used in the initial annealing temperature study (Fig. 2). The main crystallographic planes have been indexed based upon monoclinic $HfO_2$ [32]. We have identified a crystallization stage between 325 °C and 375 °C, at which point the films transition from a mostly amorphous state to a distinct crystallized structure. Notably, there is no significant change in peak intensity or peak position within the films annealed above 375 °C, whereas effective lifetimes continue to improve up to 475 °C and degrade at higher temperatures. We therefore infer that, once the film has initially crystallized, the passivation quality is not directly related to the $HfO_2$ film crystallinity. This is not unexpected as it has been established that, in general, crystallinity is not necessary to activate the passivation of dielectric films. $Al_2O_3$, for example, provides excellent passivation whilst in an amorphous state [33]. Furthermore, titanium dioxide ($TiO_2$) provides decreased passivation quality with higher annealing temperatures, as the film transitions from an anatase to rutile phase [34], [35].

### D. Understanding Field and Chemical Passivation of the Films

Kelvin probe measurements can be used to determine the work function of a material [36], which is important when considering factors like conductivity and charge carrier tunneling probability. For complex structures including dielectric layers, an "effective" work function can be used to extract information about the charge in the dielectric layer [37].

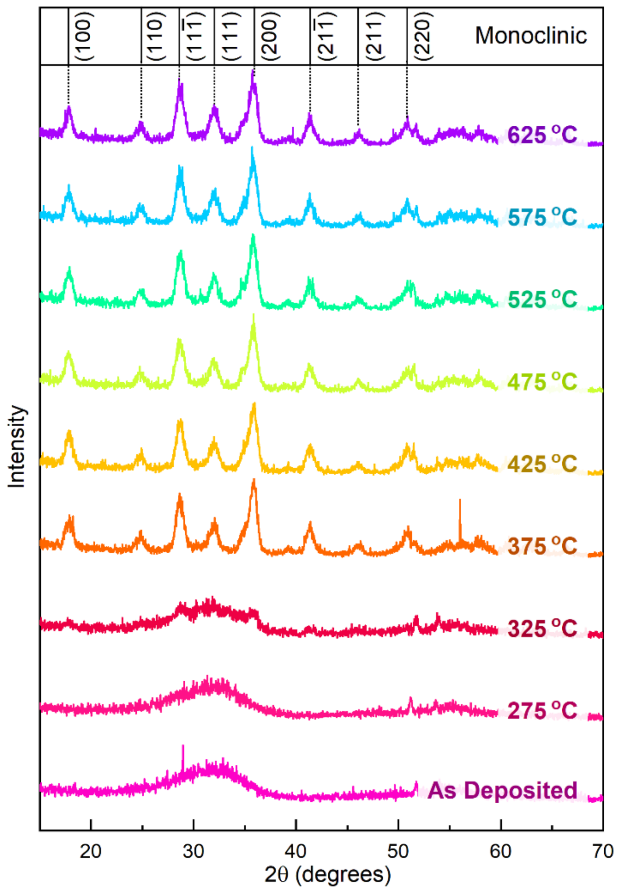


Fig. 4. GI-XRD measurements, using Cu $K_{\alpha 1/2}$, taken from polished silicon wafers coated with 12 nm (100 cycles) of $HfO_2$ grown by ALD annealed in air for 30 min at temperatures ranging from as-deposited (200 °C) to 625 °C. The main crystallographic planes present are labeled at the top. Patterns are vertically offset for clarity.

The relation between activation annealing temperature and the effective work function of 12 nm $HfO_2$ films deposited on silicon can be seen in Fig. 5(a). At low annealing temperatures, the effective work function of the $HfO_2$ films is around 4.6 eV. This remains relatively constant until the temperature reaches 375 °C, where the effective work function begins to increase up to 5.1 eV at 450 °C. The effective work function then remains relatively stable for all higher annealing temperatures investigated. Interestingly, the initial turning point roughly corresponds to the crystallization of the $HfO_2$ films, as determined *via* XRD, whereas the second turning point at 450 °C is close to the 475 °C annealing temperature which produces the best effective lifetimes. From this, we have inferred a potential link between the observed enhancement in measured lifetime and the effective work function, which may result from varying charge within the dielectric layer [37]. It is also possible that the initial shift in effective work function relates to changes within the physical structure of the $HfO_2$ layer as it crystallizes, which impact the dielectric constant. The plateau in effective work function

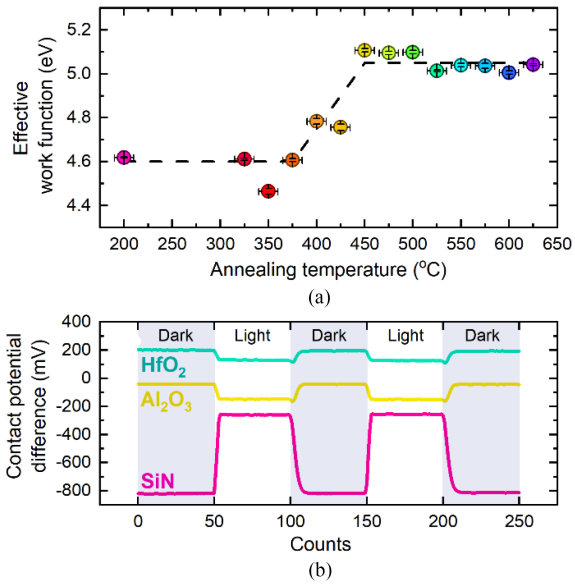


Fig. 5. (a) Effective work functions of 12 nm $HfO_2$ films deposited on 120 μm thick 5 Ωcm *n*-type Cz-Si wafers and annealed for 30 min at different temperatures, as determined from Kelvin probe measurements, with the dashed curve providing a guide to the eye (b) CPD data measured under dark and light conditions for an ALD $HfO_2$ film annealed at 475 °C, an ALD $Al_2O_3$ film annealed at 460 °C in air, and a PECVD SiN film.

at higher annealing temperatures suggests that the decrease in effective lifetime occurs because of a different mechanism than changes in the crystallinity or effective work function, and thus is likely chemical in nature.

To investigate the surface charge polarity of the $HfO_2$ films, SPV was used, which is determined by measuring the difference in CPD in the dark compared with under illumination. An example of this can be seen in Fig. 5(b), where the shaded regions represent data points measured in the dark, and nonshaded regions measured under illumination. For all annealing temperatures, the SPV of the $HfO_2$ films was negative. To support our results, we have directly compared the CPD response of our $HfO_2$ films to $Al_2O_3$ (known to have a negative charge) and $SiN_x$ (known to have a positive charge) [38]. Our results match those of Aubriet et al. [39]. Literature shows evidence for either positive [8], [11] or negative [9], [10] fixed charges in $HfO_2$ films, although the exact mechanisms through which a certain charge polarity is achieved is currently unknown. Suggestions have been made that incorporation of Cl or $N_2$ may produce a negative charge polarity [7], [13]. It is important to note that a range of different hafnium-containing precursors have been used to create $HfO_2$ films by ALD, including TDMAH [10], tetrakis(methylethylamide)hafnium (TEMAH) [11], [12], [13], [40], trimethylhafnium [9], and $HfCl_4$ [7], and this may explain variations in charge polarities reported.

To assess the magnitude of charge in our $HfO_2$ films, we have used positive corona charging of the surface to neutralize the negative fixed charge. As net charge is neutralized, field-effect passivation decreases, and thus effective lifetime decreases [40]. As further charge is deposited onto the surface of the passivating layer, the field-effect passivation and hence effective lifetime increases again. The amount of corona charge deposited onto the surface, $Q_{corona}$, which is required to reach the minimum effective lifetime, $\tau_{min}$, provides an indication of the amount of charge initially present. Since, at the minimum lifetime value, the field effect is neutralized and only chemical passivation remains, we use $\tau_{min}$ as a measure of the level of chemical passivation given by the film. It has been assumed that the capture cross sections for carrier recombination are not influenced by factors such as recrystallization and, as such, remain consistent across measurements.

Examples of corona charge curves for a 12 nm thick sample of $HfO_2$, annealed at different temperatures for 30 min in air, can be seen in Fig. 6(a). A clear minimum value can be seen for each curve, at which point the data for $Q_{corona}$ and $\tau_{min}$ are extracted. In all cases, the effective lifetime rises again as positive charge continues to be applied, as field-effect passivation of positive polarity increases. The recovery in lifetime indicates that the charge leakage is minimal over the timescales considered.

The applied positive corona charge to neutralize the negative charge within the $HfO_2$ layer, plotted in Fig. 6(b), shows a significant increase between 300 and 425 °C. The implied level of charge in the films then begins to plateau around $2 \times 10^{12}$ qcm$^{-2}$, before gradually decreasing, as the annealing temperature increases. This level of charge is broadly consistent with some previous studies, where negative $HfO_2$ is found to be on the order of $10^{11}$–$10^{12}$ qcm$^{-2}$ [7], [9], [10], [13]. Based upon the trends observed in Figs. 4, 5(a), and 6(b), it is possible that the crystallization has an influence on the effective charge density within the film and, by extension, the effective work function.

The minimum lifetime reached for each temperature is shown in Fig. 6(c), which provides an indication of the annealing temperature dependence of chemical passivation. The trend is broadly consistent with the trend in lifetime values shown in Fig. 2, with lifetimes increasing and then decreasing as annealing temperature increases. Fig. 6(c) shows that chemical passivation peaks around 425 °C. Cheng et al. [10] also found a similar temperature dependence of chemical passivation, with their density of interface states ($D_{it}$) reaching a minimum at 450 °C. This trend suggests that chemical passivation may be the dominant factor when considering the decrease in passivation quality, especially when considering the bulk lifetime of the wafers used in this study was found to increase with annealing temperature.

Using the values for $Q_{corona}$ and $\tau_{min}$ as a guideline, we have modeled the lifetime curves from Fig. 2(a) and (b). Given the injection range of these curves, it was not possible to extract exact values of $Q_f$ (the fixed charge density) and $D_{it}$. However, we were able to quantify the relative changes in these parameters between high and low lifetime curves. The passivation enhancement between 325 °C and 475 °C can be attributed to a 75% decrease in $D_{it}$ and a 100% increase in $Q_f$. Between 475 °C and 625 °C, $D_{it}$ returns toward its initial value, whereas the relative decrease in $Q_f$ is only 10%, This simulation supports our claim that passivation enhancement is a contribution of both chemical and field-effect mechanisms, and the decrease in passivation quality at higher temperatures is chemical in nature.

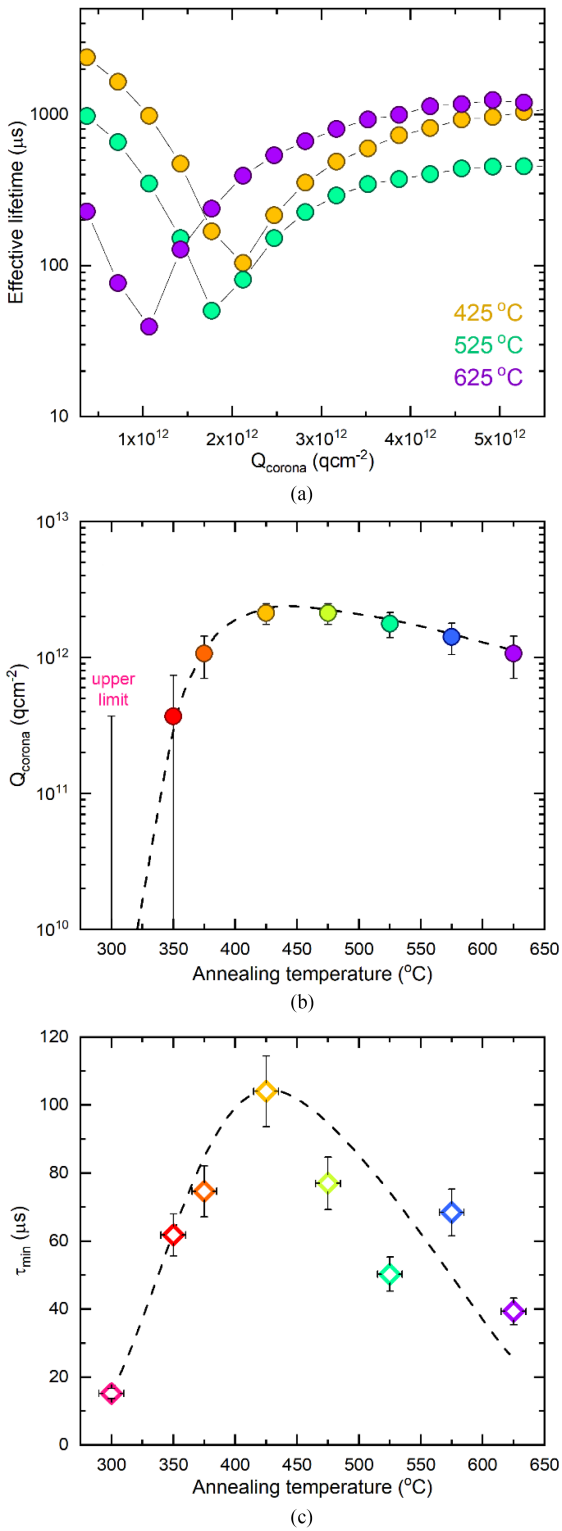


Fig. 6. (a) Corona charging curves showing effective lifetime, extracted at an excess carrier density of $1 \times 10^{15}$ cm$^{-3}$, of 12 nm $HfO_2$ passivated 150 $\mu$m 5 $\Omega$cm $n$-type Cz-Si samples as positive corona charge is increased, at a range of selected activation temperatures. (b) Positive corona charge required to minimize the effective lifetime (*i.e.*, neutralize the negative field-effect passivation), as a function of activation temperature. (c) Minimum lifetime reached during corona charging as a function of annealing temperature, which is indicative of the level of chemical passivation. The dashed curves in (b) and (c) provide a guide to the eye.

## IV. Conclusion

We have studied the mechanisms underpinning the postdeposition activation annealing conditions for $HfO_2$ films on Si deposited *via* ALD, determining a preferred annealing time of 30 min, annealing ambient of air (rather than Ar or $N_2$), and a distinct temperature dependence. Effective lifetime peaks at an annealing temperature of 475 °C, with a minimum SRV value of 4.1 cm/s and corresponding single-sided $J_0$ value of 37.1 fA/cm$^2$. Above this temperature, effective lifetime steadily decreases which, through use of room temperature superacid repassivation, has been shown not to be because of bulk lifetime degradation.

GI-XRD revealed a distinct crystallized monoclinic $HfO_2$ structure in all $HfO_2$ films annealed above 375 °C, with crystallization occurring between 325 and 375 °C. This temperature range coincides with an initial increase in measured lifetime, with further lifetime variations not corresponding to changes in film crystallinity. Kelvin probe measurements indicated a potential relationship between initial passivation enhancement and a positive effective work function shift between 375 and 450 °C. Through a combination of SPV measurements and positive corona charging, we have determined that our $HfO_2$ films have a negative charge polarity. The maximum charge density was observed after 425 °C annealing and was on the order of $2 \times 10^{12}$ qcm$^{-2}$. Analysis of the corona charging results highlighted a significant change in negative charge density within the $HfO_2$ layer as it crystallizes, with the charge density reaching its peak around the optimal annealing temperatures for best lifetime values. This was followed by a gradual decrease in negative charge as lifetime decreases at higher annealing temperatures. Investigations into chemical passivation indicated a very similar trend between chemical passivation and effective lifetime as functions of annealing temperature. Overall, the results suggest a combined contribution of chemical and field-effect mechanisms is responsible for passivation enhancement, with similar relative changes in $D_{it}$ and $Q_f$. The decrease in passivation quality at higher temperatures is likely dominated by chemical factors.

In conjunction with the well-known properties of $HfO_2$ (e.g., electrically insulating, high dielectric constant, and chemically resistant), our work has demonstrated that thin $HfO_2$ layers can provide a very high level of passivation. Understanding of passivation mechanisms in $HfO_2$ enables further investigation into enhancement of passivation quality and ultimately incorporation of $HfO_2$ into various photovoltaic architectures.

## IV. Data Access Statement

Data underpinning figures in this article can be downloaded from https://wrap.warwick.ac.uk/171645. Requests for additional data should be made directly to the corresponding author. For the purpose of open access, the author has applied a Creative Commons Attribution (CC BY) license to any Author Accepted Manuscript version arising from this submission.

## ACKNOWLEDGMENT

X-ray diffraction measurements were made using equipment provided by the University of Warwick X-ray Diffraction Research Technology Platform.

## REFERENCES

[1] R. S. Bonilla, B. Hoex, P. Hamer, and P. R. Wilshaw, "Dielectric surface passivation for silicon solar cells: A review," *Phys. Status Solidi (A) Appl. Mater. Sci.*, vol. 214, 2017, Art. no. 1700293, doi: 10.1002/pssa.201700293.

[2] H. Mulaosmanovic et al., "Ferroelectric field-effect transistors based on $HfO_2$: A review," *Nanotechnology*, vol. 32, 2021, Art. no. 502002, doi: 10.1088/1361-6528/ac189f.

[3] M. Pešić et al., "Physical mechanisms behind the field-cycling behaviour of $HfO_2$-based ferroelectric capacitors," *Adv. Funct. Mater.*, vol. 26, pp. 4601–4612, 2016, doi: 10.1002/adfm.201600590.

[4] M. Fadel, O. A. Azim M., O. A. Omer, and R. R. Basily, "A study of some optical properties of hafnium dioxide ($HfO_2$) thin films and their applications," *Appl. Phys. A: Mater. Sci. Process.*, vol. 66, pp. 335–343, 1998, doi: 10.1007/s003390050675.

[5] K. Mergia, V. Liedtke, T. Speliotis, G. Apostolopoulos, and S. Messoloras, "Thermo-mechanical behaviour of $HfO_2$ Coatings for aerospace applications," *Adv. Mater. Res.*, vol. 59, pp. 87–91, 2008, doi: 10.4028/www.scientific.net/AMR.59.87.

[6] J. S. Daubert et al., "Corrosion protection of copper using $Al_2O_3$, $TiO_2$, ZnO, $HfO_2$, and $ZrO_2$ atomic layer deposition," *ACS Appl. Mater. Interfaces*, vol. 9, pp. 4192–4201, 2017, doi: 10.1021/acsami.6b13571.

[7] R. Sreenivasan, P. C. McIntyre, H. Kim, and K. C. Saraswat, "Effect of impurities on the fixed charge of nanoscale $HfO_2$ films grown by atomic layer deposition," *Appl. Phys. Lett.*, vol. 89, 2006, Art. no. 112903, doi: 10.1063/1.2348735.

[8] J. Wang, S. S. Mottaghian, and M. F. Baroughi, "Passivation properties of atomic-layer-deposited hafnium and aluminum oxides on Si surfaces," *IEEE Trans. Electron. Devices*, vol. 59, no. 2, pp. 342–348, Feb. 2012, doi: 10.1109/TED.2011.2176943.

[9] F. Lin, B. Hoex, Y. H. Koh, J. Lin, and A. G. Aberle, "Low-temperature surface passivation of moderately doped crystalline silicon by atomic-layer-deposited hafnium oxide films," *ECS J. Solid State Sci. Technol.*, vol. 2, pp. N11–N14, 2013, doi: 10.1149/2.026301jss.

[10] X. Cheng et al., "Surface passivation properties of $HfO_2$ thin film on n-type crystalline Si," *IEEE J. Photovolt.*, vol. 7, no. 2, pp. 479–485, Mar. 2017, doi: 10.1109/JPHOTOV.2016.2645399.

[11] J. Cui et al., "Highly effective electronic passivation of silicon surfaces by atomic layer deposited hafnium oxide," *Appl. Phys. Lett.*, vol. 110, 2017, Art. no. 021602, doi: 10.1063/1.4973988.

[12] A. B. Gougam, B. Rajab, and A. Bin Afif, "Investigation of c-Si surface passivation using thermal ALD deposited $HfO_2$ films," *Mater. Sci. Semicond. Process.*, vol. 95, pp. 42–47, 2019, doi: 10.1016/j.mssp.2019.02.012.

[13] S. Tomer et al., "Silicon surface passivation by atomic layer deposited hafnium oxide films: Trap states investigation using constant voltage stress studies," *IEEE J. Photovolt.*, vol. 10, pp. 1614–1623, 2020, doi: 10.1109/JPHOTOV.2020.3022686.

[14] S. L. Pain et al., "Electronic characteristics of ultra-thin passivation layers for silicon photovoltaics," *Adv. Mater. Interfaces*, vol. 28, 2022, Art. no. 2201339, doi: 10.1002/admi.202201339.

[15] N. E. Grant et al., "Permanent annihilation of thermally activated defects which limit the lifetime of float-zone silicon," *Phys. Status Solidi (A) Appl. Mater. Sci.*, vol. 213, pp. 2844–2849, 2016, doi: 10.1002/pssa.201600360.

[16] N. E. Grant et al., "Superacid-treated silicon surfaces: Extending the limit of carrier lifetime for photovoltaic applications," *IEEE J. Photovolt.*, vol. 7, no. 6, pp. 1574–1583, Nov. 2017, doi: 10.1109/JPHOTOV.2017.2751511.

[17] A. L. Blum et al., "Interlaboratory study of eddy-current measurement of excess-carrier recombination lifetime," *IEEE J. Photovolt.*, vol. 4, no. 1, pp. 525–531, Jan. 2014, doi: 10.1109/JPHOTOV.2013.2284375.

[18] T. Niewelt et al., "Reassessment of the intrinsic bulk recombination in crystalline silicon," *Sol. Energy Mater. Sol. Cells*, vol. 235, 2022, Art. no. 111467, doi: 10.1016/j.solmat.2021.111467.

[19] D. E. Kane and R. M. Swanson, "Measurement of the emitter saturation current by a contactless decay method," in *Proc. IEEE 18th Photovolt. Specialist Conf.*, 1985, pp. 578–583.

[20] A. I. Pointon, N. E. Grant, E. C. Wheeler-Jones, P. P. Altermatt, and J. D. Murphy, "Superacid-derived surface passivation for measurement of ultra-long lifetimes in silicon photovoltaic materials," *Sol. Energy Mater. Sol. Cells*, vol. 183, pp. 164–172, 2018, doi: 10.1016/j.solmat.2018.03.028.

[21] A. I. Pointon, N. E. Grant, S. L. Pain, J. T. White, and J. D. Murphy, "Sub-2 cm/s passivation of silicon surfaces by aprotic solutions," *Appl. Phys. Lett.*, vol. 116, 2020, Art. no. 121601, doi: 10.1063/5.0003704.

[22] B. H. Toby and R. B. Von Dreele, "GSAS-II: The genesis of a modern open-source all purpose crystallogrpahy software package," *J. Appl. Crystalllography*, vol. 46, pp. 544–549, 2013, doi: 10.1107/S0021889813003531.

[23] I. D. Baikie, S. Mackenzie, P. J. Z. Estrup, and J. A. Meyer, "Noise and the Kelvin method," *Rev. Sci. Instrum.*, vol. 62, pp. 1326–1332, 1991, doi: 10.1063/1.1142494.

[24] R. S. Bonilla, F. Woodcock, and P. R. Wilshaw, "Very low surface recombination velocity in n-type c-Si using extrinsic field effect passivation," *J. Appl. Phys.*, vol. 116, 2014, Art. no. 054102, doi: 10.1063/1.4892099.

[25] R. S. Bonilla et al., "Corona charge in $SiO_2$: Kinetics and surface passivation for high efficiency silicon solar cells," *Energy Procedia*, vol. 92, pp. 326–335, 2016, doi: 10.1016/j.egypro.2016.07.090.

[26] K. R. McIntosh and L. E. Black, "On effective surface recombination parameters," *J. Appl. Phys.*, vol. 116, 2014, Art. no. 014503, doi: 10.1063/1.4886595.

[27] J. Kim, M. Ju, Y. Kim, and J. Yi, "Chemical stoichiometry effect of hafnium oxide ($HfO_x$) for passivation layer of PERC solar cells," *Mater. Sci. Semicond. Process.*, vol. 148, 2022, Art. no. 106833, doi: 10.1016/j.mssp.2022.106833.

[28] N. E. Grant et al., "Atomic level termination for passivation and functionalisation of silicon surfaces," *Nanoscale*, vol. 12, pp. 17332–17341, 2020, doi: 10.1039/d0nr03860a.

[29] G. D. Watkins, "Intrinsic defects in silicon," *Mater. Sci. Semicond. Process.*, vol. 3, pp. 227–235, 2000, doi: 10.1016/S1369-8001(00)00037-8.

[30] F. E. Rougieux, N. E. Grant, and D. Macdonald, "Thermal deactivation of lifetime-limiting grown-in point defects in n-type Czochralski silicon wafers," *Physica Status Solidi - Rapid Res. Lett.*, vol. 7, pp. 616–618, 2013, doi: 10.1002/pssr.201308053.

[31] N. E. Grant et al., "Thermal activation and deactivation of grown-in defects limiting the lifetime of float-zone silicon," *Phys. Status Solidi Rapid Res. Lett.*, vol. 10, pp. 443–447, 2016, doi: 10.1002/pssr.201600080.

[32] C. E. Curtis, L. M. Doney, and J. R. Johnson, "Some properties of hafnium oxide, hafnium silicate, calcium hafnate, and hafnium carbide," *J. Amer. Ceram. Soc.*, vol. 37, pp. 458–465, 1954, doi: 10.1111/j.1151-2916.1954.tb13977.x.

[33] M. Broas, O. Kanninen, V. Vuorinen, M. Tilli, and M. Paulasto-Kröckel, "Chemically stable atomic-layer-deposited $Al_2O_3$ films for processability," *ACS Omega*, vol. 2, pp. 3390–3398, 2017, doi: 10.1021/acsomega.7b00443.

[34] I.-S. Yu, Y.-W. Wang, H.-E. Cheng, Z.-P. Yang, and C.-T. Lin, "Surface passivation and anti-reflection behavior of ALD $TiO_2$ on n-type silicon for solar cells," *Int. J. Photoenergy*, vol. 7, 2013, Art. no. 431614, doi: 10.1155/2013/431614.

[35] T. Matsui, M. Bivour, P. F. Ndione, R. S. Bonilla, and M. Hermle, "Origin of the tunable carrier selectivity of atomic-layer-deposited $TiO_x$ nanolayers in crystalline silicon solar cells," *Sol. Energy Mater. Sol. Cells*, vol. 209, 2020, Art. no. 110461, doi: 10.1016/j.solmat.2020.110461.

[36] W. Melitz, J. Shen, A. C. Kummel, and S. Lee, "Kelvin probe force microscopy and its application," *Surf. Sci. Rep.*, vol. 66, pp. 1–27, 2011, doi: 10.1016/j.surfrep.2010.10.001.

[37] R. S. Bonilla, "Modelling of Kelvin probe surface voltage and photovoltage in dielectric-semi-conductor interfaces," *Mater. Res. Express*, vol. 9, 2022, Art. no. 085901, doi: 10.1088/2053-1591/ac84c8.

[38] R. Hezel and K. Jaeger, "Low-temperature surface passivation of silicon for solar cells," *J. Electrochem. Soc.*, vol. 136, pp. 518–523, 1989, doi: 10.1149/1.2096673.

[39] V. Aubriet, K. Courouble, M. Gros-Jean, and Ł. Borowik, "Correlative analysis of embedded silicon interface passivation by Kelvin probe force microscopy and corona oxide characterization of semiconductor," *Rev. Sci. Instrum.*, vol. 92, 2021, Art. no. 083905, doi: 10.1063/5.0052885.

[40] G. Dingemans and W. M. M. Kessels, "Aluminum oxide and other ALD materials for Si surface passivation," *ECS Trans.*, vol. 41, pp. 293–301, 2011, doi: 10.1149/1.3633680.